Nano Energy 84 (2021) 105920

Contents lists available at ScienceDirect

Nano Energy

journal homepage: http://www.elsevier.com/locate/nanoen

Full paper

Sandwich-like triboelectric nanogenerators integrated self-powered buoy for navigation safety

Hao Wang [a,1], Zhongqi Fan [b,1], Tiancong Zhao [c,1], Jiale Dong [a], Siyuan Wang [a], Yan Wang [a], Xiu Xiao [a], Changxin Liu [a], Xinxiang Pan [a], Yunpeng Zhao [b,*], Minyi Xu [a,*]

[a] Marine Engineering College, Dalian Maritime University, Dalian 116026, China
[b] State Key Laboratory of Coastal and Offshore Engineering, Dalian University of Technology, Dalian 116204, China
[c] School of Marine Engineering and Technology, Sun Yat-sen university, Guangzhou 510275, China

ARTICLE INFO

Keywords:
Triboelectric nanogenerator
Blue energy
Self-powered
Ocean buoy

ABSTRACT

Powering marine distributed buoys sustainably and cost-efficiently has always been challenging in the ocean environment. Triboelectric nanogenerators (TENG), thanks to their robustness, high efficiency and low cost in energy harvesting, has provided a novel solution to the long-term electrical power supply for a series of distributed systems (including buoys). In this study, a wave energy harvesting sandwich-like TENG (S-TENG) has been proposed. In the on-land forced motion experiments, the S-TENG yields much superior performances compared to previous tower-like TENG in terms of the power density. The studies also reveal that the electrical output increases linearly even with larger number of parallel connected S-TENG layers. Consequently, a buoy integrated with 7 parallel connected S-TENGs is studied through systematic wave basin experiments and the relevance of most hydrodynamic parameters (including wave height, frequency, direction as well as mooring system) have been revealed. The presented wave basin experiments are original in wave energy harvesting TENG research practice and prove to be very helpful in that they simulate the most close-to-real ocean environments in the lab. The studies are concluded with a 12 W high-brightness LED lit up on a navigation supporting buoy. This study has set a benchmark of achieving self-powered buoy with TENG, which can be extended to other marine distributed systems such as sensors and small robotics.

1. Introduction

As over 90% of trade in volume conducted by marine transportation and the ocean exploitation increasing rapidly, marine distributed systems are becoming more and more important [1–5]. Buoys with a variety of functions are the common marine distributed systems (such as navigation supporting buoys, a and sensor buoys). For example, navigation supporting buoys, equipped with illumination devices to be easily recognized, provide important in-place supports to navigation safety [6]. On observation that the traditional battery-powered buoys have always been accompanied by disadvantages like short service time as well as pollution risks [7,8], developing renewable energy sources to power the marine buoys is greatly preferable. Wave energy is regarded as a promising renewable energy source and it is very accessible for the scenarios of marine distributed systems [5,9–11]. Currently, wave energy harvesting is mainly performed by the electromagnetic generator (EMG) [11–13], but EMGs are not the best alternative to power every marine distributed system considering their weights, costs and efficiencies (especially when the wave frequency is relatively low) [4].

Triboelectric nanogenerator (TENG), based on coupling of triboelectrification effects and electrostatic induction, has been created to harvest ambient mechanical energy effectively [4,14–22]. Studies have shown that by extracting energy from miscellaneous sources like low-frequency wave [23], flow-induced vibration [24] or low-speed wind [25], a variety of applications can be powered by the essentially low-cost, flexible TENGs, which makes it particularly valuable for microsystems [26–28]. Recent progresses on TENG have realized some very interesting functions, such as wearable sensing [29], trajectory-tracking [30] and wireless electric energy transmission [31]. Compared with EMG, TENG yields higher output performance at low frequencies, which is practically helpful in wave energy harvesting [4, 20,32–53]. Previously, a few studies have been conducted on wave

* Corresponding authors.
E-mail addresses: ypzhao@dlut.edu.cn (Y. Zhao), xuminyi@dlmu.edu.cn (M. Xu).
[1] H. Wang, Z. Fan, T. Zhao contribute equally.

https://doi.org/10.1016/j.nanoen.2021.105920
Received 22 January 2021; Received in revised form 15 February 2021; Accepted 19 February 2021
Available online 23 February 2021

energy harvesting TENG in aspects of structure design, material treatment or system optimization. Xu et al. developed a tower-like TENG which is capable of harvesting arbitrary-directional wave energy [47], though the space utilization of the harvester could be further optimized and output performance produced by multi parallel connected units needs more investigation. Xi et al. have presented a self-powered intelligent buoy system (SIBS) powered by a multi-layered TENG. However, effects of hydrodynamic parameters such as the wave height and frequency (which have great influences) have not been studied.

In this study, a wave energy harvesting sandwich-like triboelectric nanogenerator (S-TENG) has been first proposed. Each layer of the S-TENG is compactly designed like a sandwich with two acrylic plates coated with aluminum electrode and polytetrafluoroethylene (PTFE) balls inside. Each S-TENG unit consists of 10 parallel connected layers (thanks to their stackable feature) to increase electrical output. On-land forced motion experiments reveals that the total electrical output increases linearly with the number of parallel connected S-TENG units (from 1 to 7). Based on this feature, a self-powered buoy is designed, which has integrated 7 hexagonally arranged S-TENG units (10 layers each) as the power module. The relevance of the electrical outputs to different hydrodynamic parameters (including wave frequencies, wave height, wave direction and mooring styles) is investigated systematically though wave basin experiments, which is original for a TENG integrated (self-powered) marine devices. By continuously lighting up a high-brightness LED (which is close to the function of the navigation supporting buoy), the TENG proves to be promising in achieving a self-powered marine distributed system.

2. Results and discussion

2.1. Device structure and working principle

The scenario in which the self-powered TENG buoy works as a navigation support is shown in Fig. 1a. The self-powered buoy (see Fig. 1b and c) consists of 7 hexagonally arranged S-TENG units (70 layers in total) in parallel connection as the power module, a cylindrical acrylic sealing shell (40 cm height and 35 cm diameter) as the framework structure and a clump weight as the ballast. The S-TENG units inside are of 20 cm height and 10 cm diameter and have been fixed rigidly through packing tape to make the electrical outputs in-phase (Fig. S1). At the bottom of the sealing case, a 15 kg ballast weight is deployed to balance the floating status of the self-powered buoy. The S-TENG has been designed on top of our previous work. Fig. 1d presents the schematic diagram of one layer of the S-TENG: the PTFE balls roll freely under the excitation of ocean waves which rub with two pairs of aluminum electrodes adhered on the surface of the substrate acrylic plate. The distance between the upper and lower acrylic plate is deigned to be slightly larger than the diameter (10.5 mm) of the PTFE pellet to ensure free rolling (with the help from a 3D printed brace of 10.6 mm height). Experiments have shown that the electrical output of S-TENG decreases with the distance between the upper and lower acrylic plate. As the distance increases from 10.5 mm to 13.5 mm, the transferred charge and the output current both drop slightly (around 10%). As larger distance means less chances for the PTFE balls to contact with the Al electrodes, the distance between the two plates will depress the triboelectric effects.

The working principle of the S-TENG is shown in Fig. 1e. Under the wave excitations, the PTFE balls moves freely in-between the two pairs of Aluminum electrodes. After multiple contacts with the Al electrodes, the PTFE balls will become negatively charged. Due to the electrostatic induction, an equivalent amount of positive charges will occupy the Al electrodes. As the PTFE balls move to the left/right part, positive charges are induced on the left/right electrodes. The electrons will flow (through the external circuit) from the left/right electrode to the right/left electrode, therefore a transient current is generated. Practically the S-TENG is capable of harvesting wave energy from the heave (vertical) motion as well (since the buoy moves not only horizontally but also vertically). The way it works is as the PTFE balls bounce inside, they keep contacting

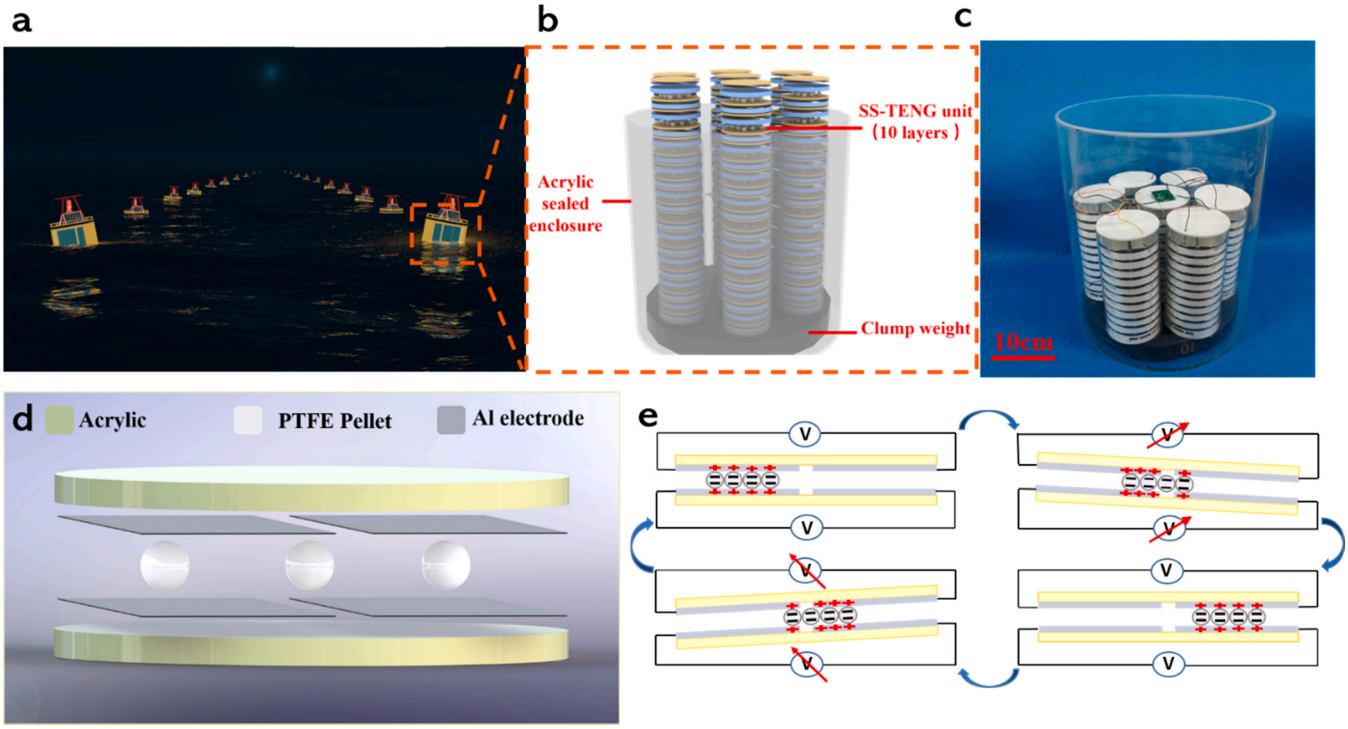

Fig. 1. The structure of the self-powered buoy and the working principle of the S-TENG. (a) The schematic diagram of the integrated self-powered buoy as navigation support along sea lanes. (b) The details of the self-powered buoy, with 7 hexagonally arranged S-TENG units (10 layers each) in parallel connection and a clump weight as ballast. (c) The photograph of the fabricated self-powered buoy. (d) The internal structure of one S-TENG layer. (e) The working principle of the S-TENG and the charge distribution in each stage.

with the upper electrodes, therefore produce electrical outputs.

2.2. Output performance of a single S-TENG Unit (10 layers)

In this subsection, the output performances of one S-TENG unit (stacked by 10 layers in parallel connection) have been studied systematically through (on-land) forced motion experiments. As shown in Fig. 2a, a linear motor is adapted to accurately force the translational motion of the TENG unit at different frequencies (0.4 Hz<f<2 Hz) and to different amplitudes (50 mm<A<130 mm). The frequency is varied from 0.4 Hz to 2 Hz to properly simulate various wave frequencies.

It is clearly shown in Fig. 2b that when the wave frequency f increases (the amplitude A is 130 mm), the short-circuit current I_{sc} increases before it reaches the maximum value of 11.94μA at 2 Hz. The transferred charge Q_{sc} yields different trend (see Fig. 2c): the transferred charge Q_{sc} increases as f increases from 0.4 Hz before it reaches the peak value of 0.70μC at 0.8 Hz. Q_{sc} remains nearly constant as f increases to 1.2 Hz but as f further increases to 2.0 Hz, Q_{sc} decreases slightly. The reason is that the natural frequency of the S-TENG unit is within the 0.8–1.2 Hz range so large Q_{sc} is achieved. As the wave frequency increases further, the output Q_{sc} decreases. It needs to be mentioned that the voltage of a whole S-TENG unit is exceeds the measurement range of a Keithley 6514 electrometer (refer to Fig. S2), therefore the voltage is not presented in Fig. 2.

The relevance of the output performance to the amplitude is shown in Fig. 2d and e. The amplitudes are simulated by the stroke distances of the linear motor. At 2 Hz frequency, it is observed that I_{sc} increases as the amplitude A increases from 50 mm to 130 mm, and I_{sc} achieves peak value of 12.28μA when A is 130 mm. Larger amplitude always indicates more energy, thus larger I_{sc} is produced through TENG. Q_{sc} remains almost constant as A increases, which indicates the PTFE balls have been fully activated and charged. By compiling a series of experiments results, Fig. 2f presents the dependence of the output current on both the amplitude and the frequency of the S-TENG. The output current of the S-TENG will be promoted with higher amplitude and frequency.

Ocean waves come from various directions so the output perfor-

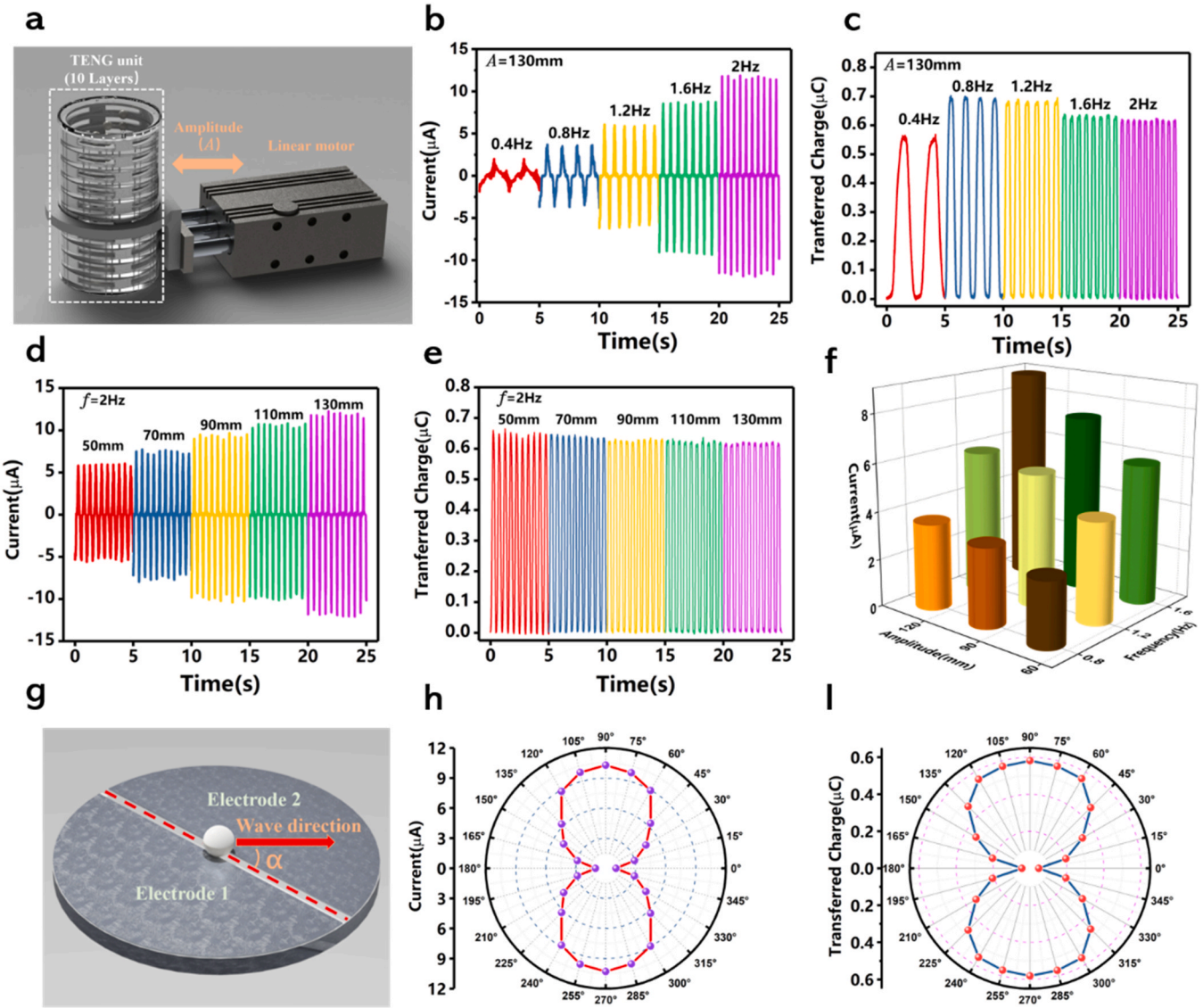

Fig. 2. The electrical output performances of one S-TENG unit (10 layers) under different wave frequencies, amplitudes and directions. (a) The schematic diagram of a single S-TENG unit moving reciprocally with the linear motor. (b) The short-circuit current I_{sc} measured under different frequencies (c)The transferred charge Q_{sc} measured under different frequencies. (d) The short-circuit current I_{sc} measured under different amplitudes (e) The transferred charge Q_{sc} measured under different amplitudes. (f) A 3D graph of the output current at different wave frequencies and amplitudes. (g) The diagram showing the angle α between the wave direction and the electrode direction. (h) The directional map of the short-circuit current I_{sc}. (i) The directional map of the transferred charge Q_{sc}.

mances under varied wave directions are studied. Fig. 2g shows the definition of the angle α between wave direction and the electrode direction. The influences of the angle α on the electrical output of S-TENG unit are shown in Fig. 2h and i. The maximum average value of I_{sc} and Q_{sc} is obtained when the angle α is 90°. That indicates the optimal electrical output is acquired when the PTFE balls moves perpendicularly to the gap of the two electrodes. As α deviates from the perpendicular direction, both I_{sc} and Q_{sc} decrease. Even when the balls moves parallel with the gap ($\alpha = 0°$), the output remains nonzero, which indicates the S-TENG can harvest wave energy from all directions (though with very different efficiencies).

In addition, the charging capabilities of an S-TENG unit with respect to different electrical parameters have also been investigated. The charging performance of different capacitors at 2 Hz frequency is shown in Fig. 3a. A 47μF capacitor could be easily charged up to 12.56 V in 300 S and the charging rate decreases with the capacitance (A 470μF capacitor could be charged to only 1.20 V in 300 S). The charging rate is also very relevant to the wave frequency (see Fig. 3b): a 100μF capacitor could be charged up to 6.73 V under 2 Hz frequency wave in 300 S, then the charging gets slower as f decreases. Higher frequency wave contains more power, leading to higher charging rate. However, there will be a top roof for the electric output as the frequency increases. At certain frequency, the transferred charge Q_{sc} and the short-circuit current I_{sc} will both reach maximum values as the charges on the PTFE balls (as the electrets) have been fully activated by the triboelectric effects.

Fig. 3c presents the output current and power density for an S-TENG unit under different loads. The power reaches its peak (25.22 mW) when the external resistance equals the internal impedance (according to Ohm's Law) while the power density reaches 34.65 W/m^3. This is an impressive improvement from our previous work on a Tower-like TENG (i.e. T-TENG), as the power density yields a significant increase (by 226.89%). On one hand, the S-TENG structure has greatly improved the utilization of inner space. On the other hand, the mechanism that two pairs of electrodes contacting with PTFE balls also increase the electrical output. The demonstration of one S-TENG unit powering a thermometer is shown in both the video demonstration Supp.V1 and Fig. 3d. A 100μF capacitor is adapted to storage electricity and to power the thermometer. Under the condition of 1 Hz wave frequency and 130 mm amplitude, after 370 s excitation, the capacitor is charged to 4.5 V, which is capable of powering a thermometer.

2.3. Output characteristic of 7 S-TENG units (70 layers)

A variety of studies have revealed that the total TENG electrical output can be promoted by increasing the number of the parallel connected TENG units. However, as the AC electrical output produced by different TENG unit has different phase, a rectifier bridge is needed in the circuit, which adds to the energy loss as well as to the circuit complexity. To secure in-phase AC output, the S-TENG structure stacks the electrodes of each layer in the same direction. We have investigated the output of multiple parallel connected TENG units as the unit number increases from 1 to 10. Additional study remains necessary as the unit number increases further may lead to floating instability, which in turn reduces the TENG's efficiency.

A forced motion platform is established to study the output characteristics of large number of parallel connected TENGs (see Fig. 4a). This platform consists of a linear motor adapted to simulate the translational motion under wave excitations. A flatbed cart (made of a 80 cm × 30 cm plank and four 1-inch straight directional wheels as a carrier) is connected with the linear motor through a 3D printed connector. 7 S-TENG units (70 layers total) are fixed rigidly (through screw) onto 7 3D printed pedestals on the flatbed cart. The electrode of each S-TENG unit is arranged to be perpendicular to the moving direction of the cart (wave direction $\alpha = 90°$) to acquire the optimal output performance, and all of the 70 S-TENG layers are connected in parallel without rectifier bridge. The corresponding equivalent circuit diagram is shown in Fig. S3. To simulate motions under real ocean wave, the frequency of the linear motor is set as 1 Hz and the amplitude is set as 130 mm. After the flatbed

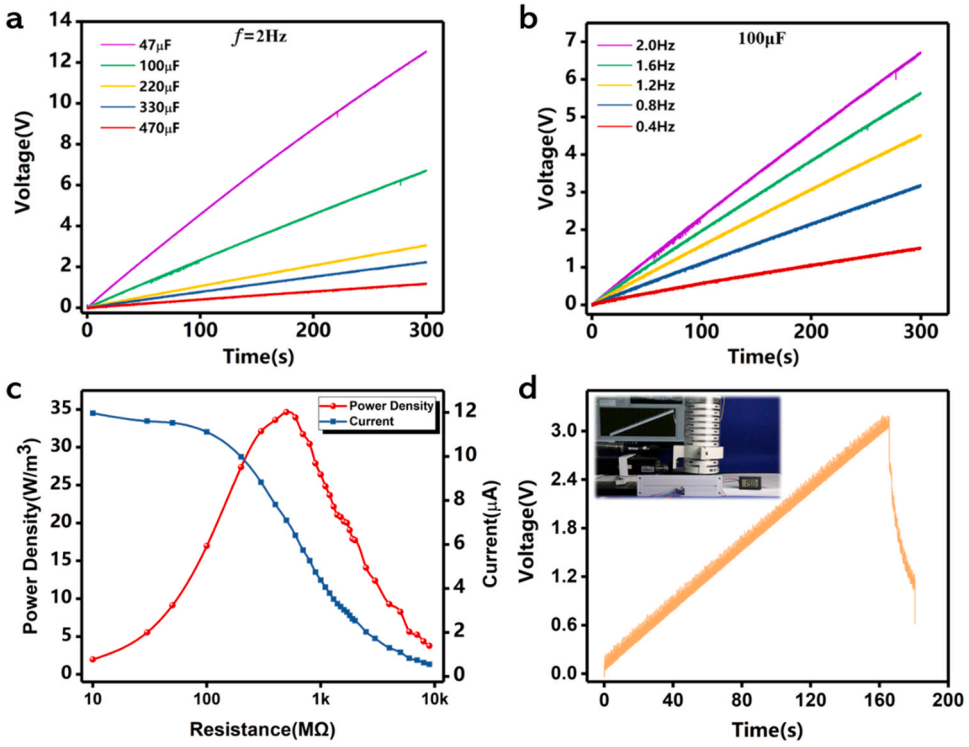

Fig. 3. The capacitor charging capability of a single S-TENG unit. (a) The diagram of a S-TENG unit charging different capacitors for 300 s under the same 2 Hz frequency. (b) The diagram of a S-TENG unit charging a same 100 μF capacitor for 300 s under different frequencies. (c) The output current and power density for a single S-TENG unit under different resistances. (d) The image of a S-TENG powering a thermometer by charging a 100μF capacitor.

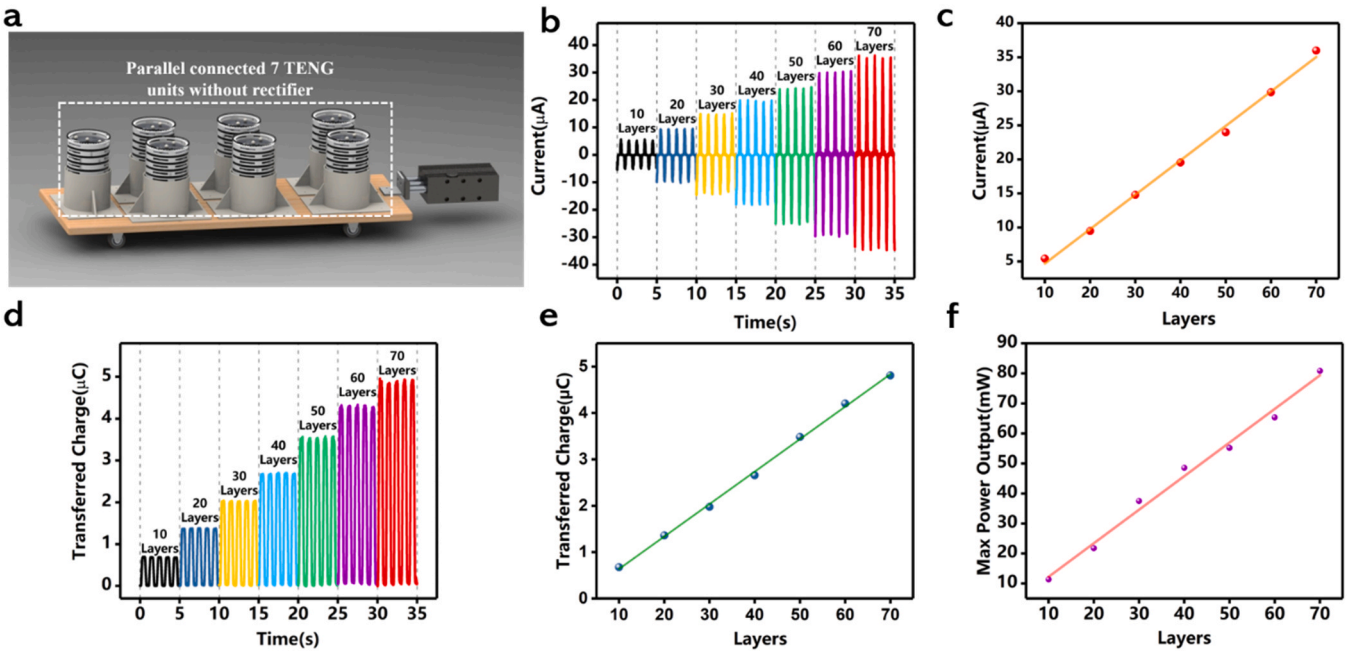

Fig. 4. Output characteristics of 7 S-TENG units (70 layers total) connected in parallel without rectifier bridge. (a) The forced motion experimental platform. (b, c) The variation of the short-circuit current I_{sc} with the number of TENG units. (d, e) The variation of the transferred charge Q_{sc} with the number of TENG units. (f) The variation of max power output with the number of TENG units.

is fully actuated, the 7 S-TENG units are connected to the circuit one by one so that the corresponding short-circuit current I_{sc} and transferred charge Q_{sc} are measured.

It is clearly shown in Fig. 4b that with the number of parallel connected S-TENG layers increasing, the average output I_{sc} increases correspondingly from 5.44 μA (10 layers), 9.48 μA (20 layers), 14.78 μA (30 layers), 19.56 μA (40 layers),23.99 μA (50 layers), 29.87 μA (60 layers) to finally 35.98 μA (70 layers). The variations of the short-circuit current I_{sc} with the number of S-TENG units (see Fig. 4c) satisfies a linear fitting. Similar to I_{sc}, the average transferred charge Q_{sc} yields an increasing trend (see Fig. 4d, 4e) with the parallel connected S-TENG units increasing from 0.68 μC (10 layers), 1.36 μC (20 layers), 1.98 μC (30 layers), 2.66 μC (40 layers), 3.48 μC (50 layers), 4.20 μC (60 layers) and finally to 4.81 μC (70 layers). The transferred charge Q_{sc} also yields linearly correlation with the number of the parallel connected S-TENGs. It's worth mentioning that the electric output yields no ceiling as the number of layer increases. Provided consistent direction of the electrodes on each layer, the output current from each layer will be in-phase (for effective superposition). Thus increasing the number of layer is an effective approach to further increase the electric output.

The dependence of the output current and power density on the number of the S-TENG units (from 1 to 7) as well as on the resistance of the load is experimentally studied. As shown in Fig. S4, the internal impedance decreases with the number of the parallel connected S-TENG units increasing. The max power output P for different parallel connected S-TENG units is calculated with the equation $P = I^2R$, where R is the internal impedance and I is the corresponding current. The variation of the maximum power output and the number of parallel connected S-TENGs appears to be linearly correlated (see Fig. 4f), which means integrating more S-TENG units together could promote the total electrical output efficiently.

2.4. Output performance of the integrated self-powered buoy in ocean engineering wave basin

As it has been verified that the electrical output will increase linearly with the number of the parallel connected S-TENG layers (from 0 to 70 layers, without a rectifier bridge), by integrating with multiple S-TENG units (as the power module), an ocean buoy is capable of sustainably converting wave energy into electricity to power itself. Thus, a self-powered buoy consists of an acrylic sealing shell, 7 hexagonally arranged S-TENG units and a clump weight is fabricated. The diameter and height of the buoy is 350 mm and 400 mm, respectively. The buoy weighs 21.58 kg, including 6.58 kg S-TENG units (0.94 kg each×7) and a 15KG shell together with the clump weight.

In order to figure out the actual (in-water) performances of the self-powered buoy, an advanced wave basin is utilized. As shown in Fig. 5a, the wave basin is of 50 m length, 3 m width and 1 m depth. A linear wave maker is located at one end of the basin while a wave damper (to eliminate the reflected waves' disturbance on the results) is located at the other end of the basin. Since the cylindrical buoy will rotate along the z axis if anchored by a single point mooring system (which disturbs the angle α between the wave direction and the electrode direction), the self-powered buoy is anchored in the middle of the basin through a double point mooring system (see Fig. 5b). However, the performances of the self-powered buoy under the single point mooring system is also experimentally studied, as shown in Fig. S5.

As far as hydrodynamics is concerned, a classical frequency-domain expression has been developed by Ogilvie et al. to describe the six degrees of freedom (surge, sway, heave, roll, pitch, and yaw) motions of a floating wave energy converter (e.g. the self-powered buoy):

$$-\omega^2\{[M]+[\mu]\}\{\xi\} - i\omega\{[B+B_{PTO}\}\{\xi\} + [K]\{\xi\} = \{f_{ex}\} \quad (1)$$

Where $\{\xi\}$ is the motion vector, $[M]$ is the mass matrix, $[\mu]$ is the added mass matrix, $[B]$ is the radiation damping matrix, $[B_{PTO}]$ is the linearized damping matrix representing the contributions from the power take-off (PTO), $[K]$ is the stiffness matrix and f_{ex} is the wave excitations. Practically, the pitch motion is the major degree of freedom that drives the translational motions of the PTFE balls in the wave basin experiments (though other degrees of freedom, like surge and heave, also make some contributions). Therefore, the decoupled pitching equation can be used to approximate the dominating motion (pitch) of the S-TENG that generates electricity:

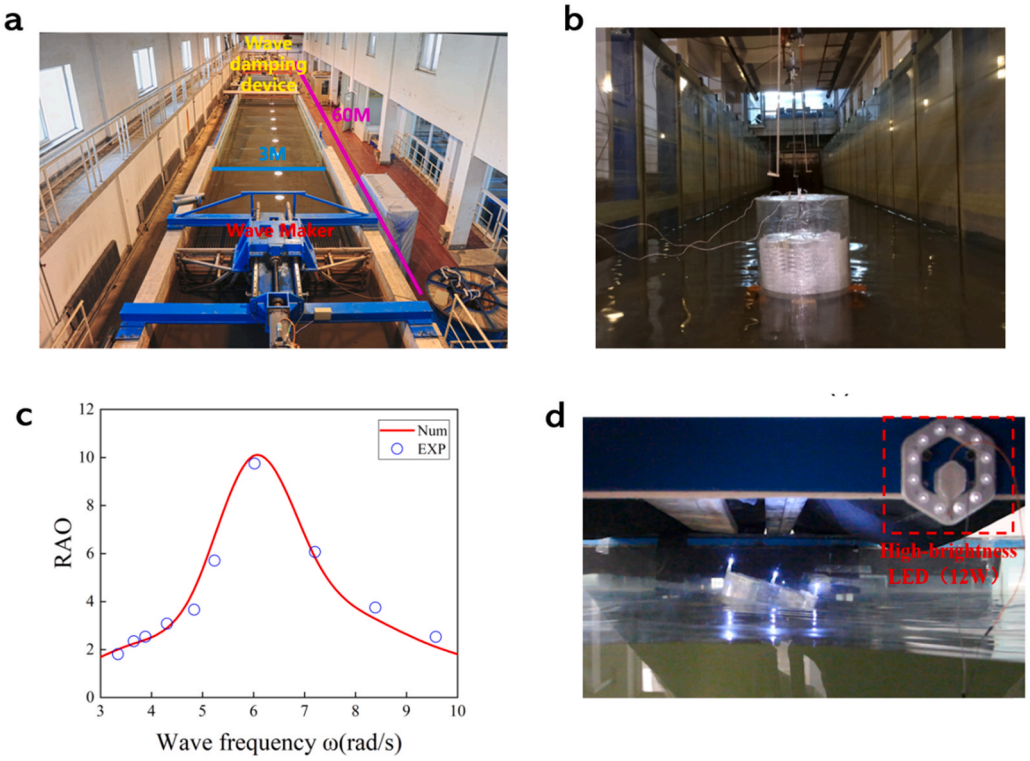

Fig. 5. The wave basin experiments of the self-powered buoy (a) The photograph of the advanced wave basin. (b) The self-powered buoy installed in the wave basin. (c) The pitch response amplitude operator (RAO) correlations between hydrodynamic analysis software and the wave basin experiments. (d) A 12 W high-brightness LED lit up by the self-powered buoy (through harvesting wav energy).

$$[M_{55}+\mu_{55}(\omega)]\ddot{\xi}_5+[B_{55}(\omega)+B_{PTO}]\dot{\xi}_5+K_{55}\xi_5=f_{ex,55}(\omega) \tag{2}$$

By taking the complex expression for the harmonic motion $\xi = A\cdot e^{(i\omega t+\theta)}$ and the complex expression for the harmonic velocity $\dot{\xi}=i\omega A\cdot e^{(i\omega t+\theta)}$ into Eq. (2), the decoupled pitching velocity can be written as:

$$\dot{\xi}_5=i\omega\xi_5=\frac{f_{ex,55}(\omega)}{i\left[\omega(M_{55}+\mu_{55})-\frac{K_{55}}{\omega}\right]-(B_{55}+B_{PTO})} \tag{3}$$

It can be observed that the pitch amplitude will become maximum when $\omega(M_{55}+\mu_{55})=\frac{K_{55}}{\omega}$, which yields the natural frequency $\omega_{5,n}$ of the floating body:

$$\omega_{5,n}=\sqrt{\frac{K_{55}}{M_{55}+\mu_{55}}} \tag{4}$$

According to Eqs. (3) and (4), when the device resonates, the velocity of the device will be in phase with the wave exciting force. The response amplitude operator (RAO), the ratio between the response amplitude and the input amplitude, for the pitch motion of the self-powered buoy can be evaluated as:

$$RAO=\frac{|\xi_5|}{A_{wave}}=\frac{f_{ex,55}(\omega)}{|-\omega^2(M_{55}+\mu_{55})-i\omega(B_{55}+B_{PTO})+K_{55}|} \tag{5}$$

The industry standard hydrodynamic software, ANSYS AQWA, has been employed to analyze the motion of self-powered buoy. The numerical results are correlated with the model tests: as shown in Fig. 5c, the pitch motions at 10 wave frequencies (from 3.34 rad/s to 9.52 rad/s) have been measured in the experiments. The natural pitching frequency of the buoy is 6.03 rad/s (0.96 Hz), which is consistent with the RAO depicted in Fig. 5c. The numerical RAOs are slightly higher than the experimental RAOs around the natural frequency. This is because sometimes the viscous damping correction in the numerical model is slightly lower than the (experimental) viscous damping when incident wave is present. However, the viscous damping we have applied was achieved from the (calm water) free decay test in the basin, which is the standard, most reliable practice to determine the viscous damping corrections in current hydrodynamics.

Wave basin experiments have demonstrated clearly the practical power generation capacity of the self-powered buoy integrated with 7 S-TENG units. This is the first time for a TENG integrated buoy to be tested comprehensively (under multiple sea states and two mooring systems) in an advanced wave basin. The wave basin is the core test facility for the State Key Laboratory of Coastal and Offshore Engineering of China. The waves are generated by the hydro-servo irregular wave maker system that provides high precision, while the wave damping on the other end of the wave basin to effectively eliminate the disturbance from the otherwise reflected waves. It is worth mentioning the actual operations are usually accompanied by issues unexpected before the wave basin tests. Mooring is one of the critical issues in the ocean as most of the floating systems are positioned by the corresponding mooring system. In fact, when the buoy is moored by a sign single mooring line system, parametric wave excitation will induce dynamic instabilities (in this case, unexpected yaw around the z-axis). This phenomenon was eliminated (to make the measurement clearer but it can be also utilized) after two-line mooring system was adopted.

Under the wave generated by the wave maker to simulate the actual ocean scenario, a 12 W high-brightness LED (1 W each) is lit up by the buoy (see Fig. 5d and the video demonstration Supp.V2). It indicates that self-power could be realized with the S-TENG for a small but practical marine distributed system (since illumination device takes the majority, if not all, of the power of the navigation supporting buoy). Similar studies should be extended to other small marine distributed systems such as sensor buoys and intelligent robotics. In fact, that the majority of the marine sensors work with similar power ranging from 10^{-2} W (e.g. wave logger ~ 0.01 W, sonic wave sensor ~ 0.02 W) to 10^{0}

W (e.g. pressure sensor ~ 0.7 W, low-cost sensor buoy system ~ 2.5 W), the essentially robust and cost efficient S-TENG is a competitive approach to achieve battery independence for them.

To study how the output performance of the self-powered buoy varies with different wave parameters, a series of experiments are carried out in the wave basin. As the natural frequency of the self-powered buoy is 6.03 rad/s(0.96 Hz), the wave frequencies selected for the wave basin tests (0.77 Hz, 0.96 Hz, 1.15 Hz, 1.33 Hz and 1.52 Hz) are around the natural frequency. The experiments adopt linear waves of either 4 cm height or 6 cm height. The optimal electrical output is acquired at the wave frequency of 0.96 Hz with the wave height of 6 cm (as expected see Fig. 5a and b). The maximum short-circuit current I_{sc} reaches 20.91 μA and the maximum transferred charge Q_{sc} reaches 2.22 μC, which is quite desirable for a wave energy harvesting TENG. Fig. 6.

The electrical outputs under different wave heights are shown in Fig. 5c and d, in which the wave maker generate waves with the same frequency of 0.96 Hz but different heights. It turns out that the average output I_{sc} under the of 4 cm wave is 17.01μA, lower than the average output I_{sc} 18.75 μA under 6 cm wave. But the average output Q_{sc} under 4 cm and 6 cm wave height condition turns out to be fairly close (2.18 μC and 2.16 μC). The reason is that larger wave height accompanies higher velocity to induce larger short-circuit current. However, either 4 cm height or 6 cm height wave have fully driven the maximum charges from the rolling PTFE balls. Therefore, no obvious difference in output Q_{sc} can be observed. This is consistent with what we have found from the single S-TENG unit's forced motion experiments.

Fig. 5e and f show the electrical outputs at different wave frequencies. Though the output I_{sc} is relatively small at the frequency of 0.77 Hz, I_{sc} can be maximized as f increases to 0.96 Hz (the natural frequency of the buoy). After the natural frequency, as the wave frequency increases, the output I_{sc} decreases. The output Q_{sc} under different wave frequencies yields similar trend: the maximum output Q_{sc} is acquired at the natural frequency of the buoy (0.96 Hz) though the output Q_{sc} remains almost same as wave frequency increases to 1.15 Hz. As the wave frequency increases further, the output Q_{sc} gradually decreases. This can be explained by the fact that when the self-powered buoy resonates under the wave excitation, the most intensive pitch motion drives the S-TENG to the maximum electrical output. However, it's determined by the characteristic of the S-TENG that once it is fully activated, the output transferred charge will have no major variation.

3. Conclusions

In this study, a sandwich-like triboelectric nanogenerator (S-TENG) for wave energy harvesting has been proposed. This compact S-TENG (with PTFE pellets inside two acrylic plates coated with aluminum electrode), can be easily stacked into parallel connection. The S-TENG is investigated through systematic on-land forced motion experiments while an S-TENG integrated is first investigated through systematic wave basin experiments.

In the forced-motion experiments, the produced power density of S-TENG reaches 34.65 W/m^3, which records a 226% increase from the previously studies T-TENG. In addition, the total electrical output increases linearly with the number of the parallel connected S-TENG units (up to 70 layers). This characteristic actually forms the basis of a self-powered buoy (as the electrical output could be promoted by simply integrating more TENG layers). Consequently, a self-powered buoy consisting 7 hexagonally arranged S-TENG units is fabricated and tested in an advanced wave basin. The optimal electrical output of the self-powered buoy is achieved when the wave frequency matches the buoy's natural (pitching) frequency: the short-circuit current can reach 20.91μA while the transferred charge can reach 2.22μC. It means that the generated electricity is capable of lighting up a 12 W high-brightness LED directly. The S-TENG integrated buoy has set a benchmark of achieving self-powered marine devices, which is critical to a series of marine agenda including promoting navigation safety at sea lanes.

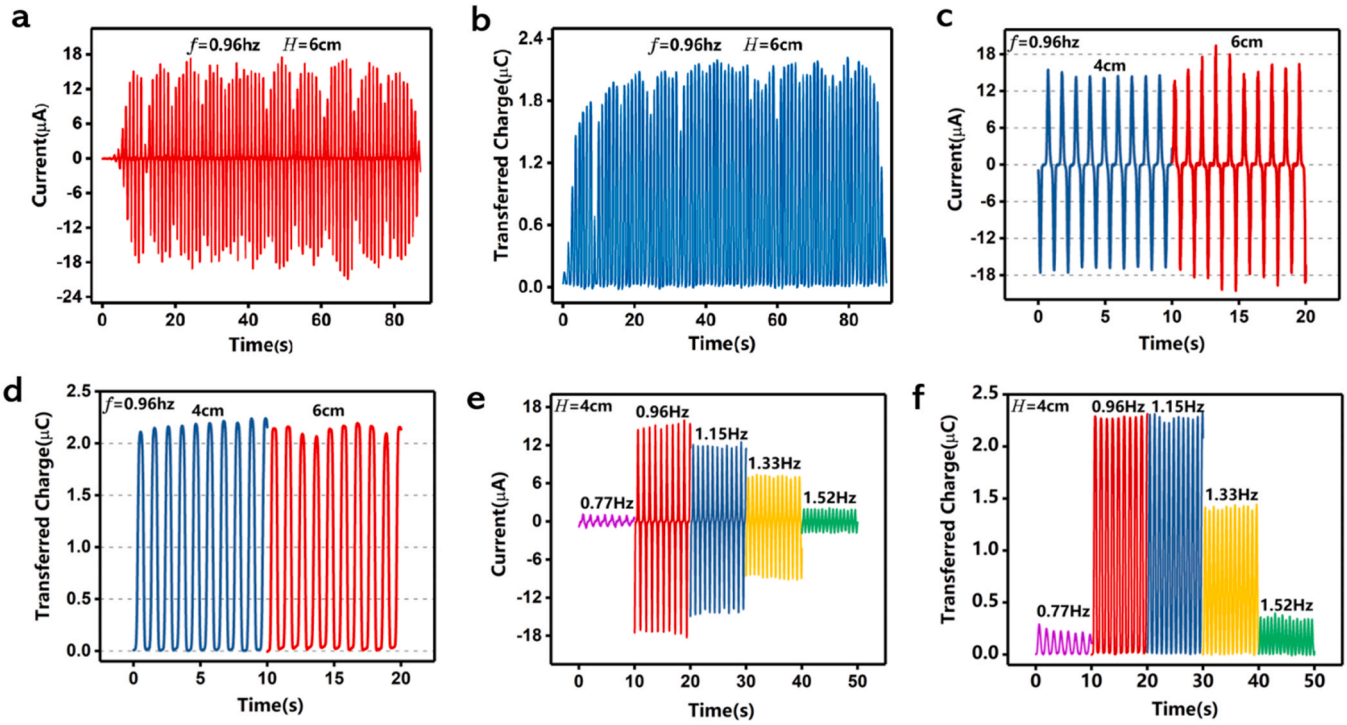

Fig. 6. Studies of performance sensitivity to the hydrodynamic parameters. (a) The photograph of the wave basin and the self-powered buoy installed in the basin. (a) The short-circuit current I_{sc} under 0.96 Hz wave frequency and 6 cm wave height. (b) The transferred charge Q_{sc} under 0.96 Hz wave frequency and 6 cm wave height. (c) The short-circuit current I_{sc} under different wave heights. (d) The transferred charge Q_{sc} under different wave heights. (e) The short-circuit current I_{sc} at different wave frequencies. (f) The transferred charge Q_{sc} at different wave frequencies.

4. Experimental methods

4.1. Fabrication of S-TENG unit

The acrylic plate of a single layer S-TENG is of 5 mm thickness and 10 cm diameter. Two aluminum electrodes with a thickness of 50 μm and an area of 6 cm × 4 cm are parallel attached onto two sides of the acrylic plate. PTFE balls with 10.5 mm diameter are filled between two acrylic plates and they are produced by 3 M company. Each S-TENG unit consists of 10 layers stacked S-TENG in parallel connection and acrylic block shell. The acrylic block shell has 10 cm diameter and 20 cm height. There are four AC output copper ends in an S-TENG unit, one pair at the top and the other pair at the bottom.

4.2. Fabrication of self-powered buoy

The buoy consists of 7 S-TENG units as the power module, an iron plate as the ballast and an acrylic shell as the frame structure. The S-TENG units integrated inside are in parallel connection to make the AC electrical output in-phase and the they are fixed through packing tape. The ballast iron plate is 15KG with 30 cm diameter and 5 cm thickness. The acrylic shell (with 40 cm height and 35 cm diameter) consists of a cover on the top of a barrel. The gap between the barrel and the cover is sealed by PTFE tape. At the bottom of the acrylic two stainless steel mooring hooks are attached with 3 M VHB tape.

4.3. Characterizations and measurements

A Keithley 6514 system electrometer is employed for measuring the short-circuit current I_{sc} and the transferred charge Q_{sc}. (but not the open-circuit voltage of a S-TENG unit as it is beyond the range of Keithley 6514). An adjustable speed linear motor (US-52) has been adopted to perform the forced motion experiments. The charging and discharging performance of S-TENG unit was measured using a commercial thermometer and a capacitor (100 μF, 25 V). The advanced wave basin belongs to the State Key Laboratory of Coastal and Offshore Engineering, Dalian University of Technology.

CRediT authorship contribution statement

Hao Wang: Conceptualization, Methodology, Writing - original draft. **Zhongqi Fan**: Experiments performing, Formal analysis, Data curation. **Tiancong Zhao**: Formal analysis, Software, Visualization. **Jiale Dong**: Experiments performing, Writing - original draft, Data curation. **Siyuan Wang**: Software, Experiments performing. **Yan Wang**: Methodology, Investigation. **Xiu Xiao**: Writing - review & editing. **Changxin Liu**: Writing - review & editing. **Xinxiang Pan**: Validation. **Yunpeng Zhao**: Funding acquisition, Supervision. **Minyi Xu**: Funding acquisition, Conceptualization, Supervision.

Declaration of Competing Interest

The authors declare that they have no known competing financial interests or personal relationships that could have appeared to influence the work reported in this paper.

Acknowledgments

The authors are grateful for the joint support from the National Natural Science Foundation of China (Grant Nos. 51879022, 51822901, 51979045, 51906029), the Fundamental Research Funds for the Central Universities, China (Grant No. 3132019330).

Appendix A. Supporting information

Supplementary data associated with this article can be found in the online version at doi:10.1016/j.nanoen.2021.105920.

References

[1] K. Liu, Y. Liu, Z. Yang, M. Li, Z. Guo, Y. Guo, F. Hong, X. Yang, Y. He, Y. Feng, Oceansense: monitoring the sea with wireless sensor networks, ACM SIGMOBILE Mob. Comput. Commun. Rev. 14 (2) (2010) 7–9.
[2] S. Kroger, R.J. Law, Sensing the sea, Trends Biotechnol. 23 (5) (2005) 250–256.
[3] K. Alverson, D.J. Baker, Taking the pulse of the oceans, Science 314 (5806) (2006) 1657.
[4] G. Xu, W. Shen, X. Wang, Applications of wireless sensor networks in marine environment monitoring: a survey, Sensors 14 (9) (2014) 16932–16954.
[5] Z.L. Wang, T. Jiang, L. Xu, Toward the blue energy dream by triboelectric nanogenerator networks, Nano Energy 39 (2017) 9–23.
[6] A. Mills, From buoys to boats HB-LED for navigation, III-Vs Rev. 16 (8) (2003) 34–35.
[7] Q. Schiermeier, J. Tollefson, T. Scully, Electricity without carbon, Nature 454 (2008) 816–823.
[8] W. K. G. Seah, Z.A. Eu, H.-P. Tan, Wireless sensor networks powered by ambient energy harvesting (WSN-HEAP) – Survey and challenges. In 2009 1st International Conference on Wireless Communication, Vehicular Technology, Information Theory and Aerospace & Electronic Systems Technology, 2009, 1–5.
[9] J. Scruggs, P. Jacob, Harvesting ocean wave energy, Science 323 (5918) (2009) 1176–1178.
[10] Z.L. Wang, Catch wave power in floating nets, Nature 542 (7640) (2017) 159–160.
[11] J. Tollefson, Power from the oceans: blue energy, Nature 508 (7496) (2014) 302–304.
[12] A.J.R. Westwood, Ocean power: wave and tidal energy review, Refocus 5 (5) (2004) 50–55.
[13] A.F. d O. Falcão, Wave energy utilization: a review of the technologies, Renew. Sustain. Energy Rev. 14 (3) (2010) 899–918.
[14] Z.L. Wang, Triboelectric nanogenerators as new energy technology for self-powered systems and as active mechanical and chemical sensors, ACS Nano 7 (11) (2013) 9533–9557.
[15] Z.L. Wang, Triboelectric nanogenerators as new energy technology and self-powered sensors – principles, problems and perspectives, Faraday Discuss. 176 (2014) 447–458.
[16] S. Wang, L. Lin, Z.L. Wang, Triboelectric nanogenerators as self-powered active sensors, Nano Energy 11 (2015) 436–462.
[17] Z.L. Wang, On Maxwell's displacement current for energy and sensors: the origin of nanogenerators, Mater. Today 20 (2) (2017) 74–82.
[18] Z.L. Wang, Nanogenerators, self-powered systems, blue energy, piezotronics and piezo-phototronics – a recall on the original thoughts for coining these fields, Nano Energy 54 (2018) 477–483.
[19] J. Luo, Z.L. Wang, Recent advances in triboelectric nanogenerator based self-charging power systems, Energy Storage Mater. 23 (2019) 617–628.
[20] M. Mariello, F. Guido, V.M. Mastronardi, M.T. Todaro, D. Desmaële, M. De Vittorio, Nanogenerators for harvesting mechanical energy conveyed by liquids, Nano Energy 57 (2019) 141–156.
[21] C. Wu, A.C. Wang, W. Ding, H. Guo, Z.L. Wang, Triboelectric nanogenerator: a foundation of the energy for the new era, Adv. Energy Mater. 9 (1) (2019), 1802906.
[22] C. Rodrigues, D. Nunes, D. Clemente, N. Mathias, J. Correia, P. Santos, F. Taveira-Pinto, T. Morais, A. Pereira, J. Ventura, Emerging triboelectric nanogenerators for ocean wave energy harvesting: state of the art and future perspectives, Energy Environ. Sci. 13 (2020) 2657–2683.
[23] Y. Wu, Q. Zeng, Q. Tang, W. Liu, G. Liu, Y. Zhang, J. Wu, C. Hu, X. Wang, A teeterboard-like hybrid nanogenerator for efficient harvesting of low-frequency ocean wave energy, Nano Energy 67 (2020), 104205.
[24] Q. Zeng, Y. Wu, Q. Tang, W. Liu, J. Wu, Y. Zhang, G. Yin, H. Yang, S. Yuan, D. Tan, C. Hu, X. Wang, A high-efficient breeze energy harvester utilizing a full-packaged triboelectric nanogenerator based on flow-induced vibration, Nano Energy 70 (2020), 104524.
[25] Y. Zhang, Q. Zeng, Y. Wu, J. Wu, S. Yuan, D. Tan, C. Hu, X. Wang, An Ultra-durable windmill-like hybrid nanogenerator for steady and efficient harvesting of low-speed wind energy, Nano-Micro Lett. 12 (2020) 175.
[26] X. Zhang, M. Han, B. Kim, J. Bao, J. Brugger, H. Zhang, All-in-one self-powered flexible microsystems based on triboelectric nanogenerators, Nano Energy 47 (2018) 410–426.
[27] Y. Chen, D. Liu, S. Wang, Y. Li, X. Zhang, Self-powered smart active RFID tag integrated with wearable hybrid nanogenerator, Nano Energy 64 (2019), 103911.
[28] Y. Ba, J. Bao, H. Deng, Z. Wang, X. Li, T. Gong, W. Huang, X. Zhang, Single-layer triboelectric nanogenerators based on ion-doped natural nanofibrils, ACS Appl. Mater. Interfaces 12 (38) (2020) 42859–42867.
[29] D. Wen, X. Liu, H. Deng, D. Sun, H. Qian, J. Brugger, X. Zhang, Printed silk-fibroin-based triboelectric nanogenerators for multi-functional wearable sensing, Nano Energy 66 (2019), 104123.
[30] Y. Ba, J. Bao, Z. Wang, H. Deng, D. Wen, X. Zhang, C. Tu, X. Zhang, Self-powered trajectory-tracking microsystem based on electrode-miniaturized triboelectric nanogenerator, Nano Energy 82 (2021), 105730.
[31] G. Liu, J. Chen, Q. Tang, L. Feng, H. Yang, J. Li, Y. Xi, X. Wang, C. Hu, Wireless electric energy transmission through various isolated solid media based on triboelectric nanogenerator, Adv. Energy Mater. 8 (14) (2018), 1703086.

[32] S. Niu, Y.S. Zhou, S. Wang, Y. Liu, L. Lin, Y. Bando, Z.L. Wang, Simulation method for optimizing the performance of an integrated triboelectric nanogenerator energy harvesting system, Nano Energy 8 (2014) 150–156.
[33] X. Wang, S. Niu, Y. Yin, F. Yi, Z. You, Z.L. Wang, Triboelectric nanogenerator based on fully enclosed rolling spherical structure for harvesting low-frequency water wave energy, Adv. Energy Mater. 5 (24) (2015), 1501467.
[34] X. Wang, Z. Wen, H. Guo, C. Wu, X. He, L. Lin, X. Cao, Z.L. Wang, Fully packaged blue energy harvester by hybridizing a rolling triboelectric nanogenerator and an electromagnetic generator, ACS Nano 10 (12) (2016) 11369–11376.
[35] Q. Shi, H. Wang, H. Wu, C. Lee, Self-powered triboelectric nanogenerator buoy ball for applications ranging from environment monitoring to water wave energy farm, Nano Energy 40 (2017) 203–213.
[36] X. Li, J. Tao, X. Wang, J. Zhu, C. Pan, Z.L. Wang, Networks of high performance triboelectric nanogenerators based on liquid-solid interface contact electrification for harvesting low-frequency blue energy, Adv. Energy Mater. 8 (21) (2018), 1800705.
[37] T.X. Xiao, T. Jiang, J.X. Zhu, X. Liang, L. Xu, J.J. Shao, C.L. Zhang, J. Wang, Z. L. Wang, Silicone-based triboelectric nanogenerator for water wave energy harvesting, ACS Appl. Mater. Interfaces 10 (4) (2018) 3616–3623.
[38] T.X. Xiao, X. Liang, T. Jiang, L. Xu, J.J. Shao, J.H. Nie, Y. Bai, W. Zhong, Z.L. Wang, Spherical triboelectric nanogenerators based on spring-assisted multilayered structure for efficient water wave energy harvesting, Adv. Funct. Mater. 28 (35) (2018), 1802634.
[39] L. Xu, T. Jiang, P. Lin, J.J. Shao, C. He, W. Zhong, X.Y. Chen, Z.L. Wang, Coupled triboelectric nanogenerator networks for efficient water wave energy harvesting, ACS Nano 12 (2) (2018) 1849–1858.
[40] S.L. Zhang, M. Xu, C. Zhang, Y.-C. Wang, H. Zou, X. He, Z. Wang, Z.L. Wang, Rationally designed sea snake structure based triboelectric nanogenerators for effectively and efficiently harvesting ocean wave energy with minimized water screening effect, Nano Energy 48 (2018) 421–429.
[41] W. Zhong, L. Xu, X. Yang, W. Tang, J. Shao, B. Chen, Z.L. Wang, Open-book-like triboelectric nanogenerators based on low-frequency roll-swing oscillators for wave energy harvesting, Nanoscale 11 (2019) 7199–7208.
[42] P. Cheng, H. Guo, Z. Wen, C. Zhang, X. Yin, X. Li, D. Liu, W. Song, X. Sun, J. Wang, Z.L. Wang, Largely enhanced triboelectric nanogenerator for efficient harvesting of water wave energy by soft contacted structure, Nano Energy 57 (2019) 432–439.
[43] R. Lei, H. Zhai, J. Nie, W. Zhong, Y. Bai, X. Liang, L. Xu, T. Jiang, X. Chen, Z. L. Wang, Butterfly-inspired triboelectric nanogenerators with spring-assisted linkage structure for water wave energy harvesting, Adv. Mater. Technol. 4 (3) (2019), 1800514.
[44] X. Liang, T. Jiang, G. Liu, T. Xiao, L. Xu, W. Li, F. Xi, C. Zhang, Z.L. Wang, Triboelectric nanogenerator networks integrated with power management module for water wave energy harvesting, Adv. Funct. Mater. 29 (41) (2019), 1807241.
[45] J. Wang, L. Pan, H. Guo, B. Zhang, R. Zhang, Z. Wu, C. Wu, L. Yang, R. Liao, Z. L. Wang, Rational structure optimized hybrid nanogenerator for highly efficient water wave energy harvesting, Adv. Energy Mater. 9 (8) (2019), 1802892.
[46] F. Xi, Y. Pang, G. Liu, S. Wang, W. Li, C. Zhang, Z.L. Wang, Self-powered intelligent buoy system by water wave energy for sustainable and autonomous wireless sensing and data transmission, Nano Energy 61 (2019) 1–9.
[47] M. Xu, T. Zhao, C. Wang, S.L. Zhang, Z. Li, X. Pan, Z.L. Wang, High power density tower-like triboelectric nanogenerator for harvesting arbitrary directional water wave energy, ACS Nano 13 (2) (2019) 1932–1939.
[48] X. Yang, L. Xu, P. Lin, W. Zhong, Y. Bai, J. Luo, J. Chen, Z.L. Wang, Macroscopic self-assembly network of encapsulated high-performance triboelectric nanogenerators for water wave energy harvesting, Nano Energy 60 (2019) 404–412.
[49] X. Zhang, M. Yu, Z. Ma, H. Ouyang, Y. Zou, S.L. Zhang, H. Niu, X. Pan, M. Xu, Z. Li, Z.L. Wang, Self-powered distributed water level sensors based on liquid–solid triboelectric nanogenerators for ship draft detecting, Adv. Funct. Mater. 29 (41) (2019), 1900327.
[50] H. Zhao, X. Xiao, P. Xu, T. Zhao, L. Song, X. Pan, J. Mi, M. Xu, Z.L. Wang, Dual-tube helmholtz resonator-based triboelectric nanogenerator for highly efficient harvesting of acoustic energy, Adv. Energy Mater. 9 (46) (2019), 1902824.
[51] X. Chen, L. Gao, J. Chen, S. Lu, H. Zhou, T. Wang, A. Wang, Z. Zhang, S. Guo, X. Mu, Z.L. Wang, Y. Yang, A chaotic pendulum triboelectric-electromagnetic hybridized nanogenerator for wave energy scavenging and self-powered wireless sensing system, Nano Energy 69 (2020), 104440.
[52] X. Liang, T. Jiang, Y. Feng, P. Lu, J. An, Z.L. Wang, Triboelectric nanogenerator network integrated with charge excitation circuit for effective water wave energy harvesting, Adv. Energy Mater. 10 (40) (2020), 2002123.
[53] L. Liu, Q. Shi, C. Lee, A novel hybridized blue energy harvester aiming at all-weather IoT applications, Nano Energy 76 (2020), 105052.

Hao Wang received his PhD in ocean engineering from Texas A&M University in 2020. Currently, he is an assistant professor in the Marine Engineering College of Dalian Maritime University. His research focus on the wave energy conversion, particularly through applications of triboelectric nanogenerators.

Zhongqi Fan received his B.S. degree in Port, Channel and Coastal Engineering from Changsha University of Science & Technology in 2018. Now he is a PhD candidate in School of Hydraulic Engineering, Dalian University of Technology. His research interests are focused on ocean energy devices and triboelectric nanogenerators.

Tiancong Zhao received the M.S. degree from the School of Dalian Maritime University, China., in 2017. He is currently pursuing the PhD degree at Sun Yat-sen University, China. His research interests focus on energy harvesters.

Jiale Dong is currently pursuing his master degree in Dalian Maritime University, China. His current research interests include blue energy harvesting, self-powered systems and triboelectric nanogenerators.

Siyuan Wang is currently pursuing his doctor degree in Dalian Maritime University, China. His current research interests include bionic sensor, marine sensing, self-powered systems and triboelectric nanogenerators.

Yan Wang is currently pursuing his doctor degree in Dalian Maritime University, China. His current research interests include flow induced vibration, blue energy, self-powered systems and triboelectric nanogenerators.

Dr. Xiu Xiao graduated from Tsinghua University in 2017. She was a visiting scholar at Purdue University during 2014–2016. Now she is an assistant professor in the Marine Engineering college, Dalian Maritime University. Her current research is mainly focused on new energy and its applications.

Changxin Liu, received his PhD degree from Dalian University of Technology in 2014. Now he is a lecturer in the Marine Engineering College, Dalian Maritime University. His current research is mainly focused on the areas of blue energy, self-powered systems, compound energy harvesting, triboelectric nanogenerators, micro thermoelectric power generation and their practical applications in smart ship and ocean.

Pan Xinxiang received his B.E and PhD degrees from Marine Engineering College, Dalian Maritime University, China, in 1987 and 1999. He now is President of Guangdong Ocean University. His research interests include smart and green ship, ocean engineering, energy saving and emission reduction, ship safety and pollution control, microfluidic chip, nano energy and self-powered systems.

Prof. Yunpeng Zhao received his PhD degree in Port, Coastal and Offshore Engineering from Dalian University of Technology in 2007. Now he is a Professor in the School of Hydraulic Engineering, Dalian University of Technology. His current research is mainly focused on the numerical analysis and testing of offshore aquaculture systems, ocean energy devices and triboelectric nanogenerators.

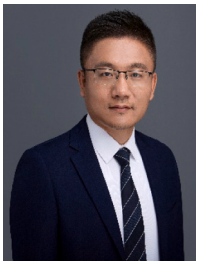

Prof. Minyi Xu received his PhD degree from Peking University in 2012. During 2016–2017, he joined Professor Zhong Lin Wang' group at Georgia Institute of Technology. Now he is a Professor in the Marine Engineering College, Dalian Maritime University. His current research is mainly focused on the areas of blue energy, self-powered systems, triboelectric nanogenerators and its practical applications in smart ship and ocean.